

# Simplest Neutral Singlet C<sub>2</sub>E<sub>4</sub> (E = Al, Ga, In, and Tl) Global Minima with Double Planar Tetracoordinate Carbons: Equivalence of C<sub>2</sub> Moieties in C<sub>2</sub>E<sub>4</sub> to Carbon Centers in CAI<sub>4</sub><sup>2-</sup> and CAI<sub>5</sub><sup>+</sup>

Yan-Bo Wu,<sup>\*,†,‡</sup> Hai-Gang Lu,<sup>†</sup> Si-Dian Li,<sup>†</sup> and Zhi-Xiang Wang<sup>\*,‡</sup>

*Institute of Molecular Science, the Key Laboratory of Chemical Biology and Molecular Engineering of Education Ministry, Shanxi University, Taiyuan, 030006, Shanxi, People's Republic of China and College of Chemistry and Chemical Engineering, Graduate University of Chinese Academy of Sciences, Beijing, 100049, People's Republic of China*

*Received: November 11, 2008; Revised Manuscript Received: January 13, 2009*

Ab initio and DFT calculations have been carried out to search for the simplest neutral singlet species with double planar tetracoordinate carbons (dptCs) [the “simplest” means the species containing the least number (six) and types (two) of atoms]. Under the restrictions to the possible models (M1–M4) with dptCs and to the singlet electronic states, the B3LYP/6–31+G\* scanning on the candidates, C<sub>2</sub>E<sub>4</sub> (E = the second- and third-row main group elements), only led to two minima (*D*<sub>2h</sub> C<sub>2</sub>Al<sub>4</sub> and *C*<sub>2h</sub> C<sub>2</sub>Be<sub>4</sub>) with stable DFT wave functions. The extensions to the heavier elements after the fourth row in the IIA and IIIA groups revealed that the *D*<sub>2h</sub> C<sub>2</sub>E<sub>4</sub> (E = Ga, In, and Tl) are also minima with dptCs but C<sub>2</sub>Ca<sub>4</sub> (*C*<sub>2h</sub>) is a first-order saddle point. Extensive explorations at the DFT level on their potential energy surfaces (PESs) further confirmed that the *D*<sub>2h</sub> C<sub>2</sub>E<sub>4</sub> (E = Al, Ga, In, and Tl) are the global minima, but the *C*<sub>2h</sub> C<sub>2</sub>Be<sub>4</sub> is a local minimum. The optimizations at the MP2 level distorted the *D*<sub>2h</sub> C<sub>2</sub>E<sub>4</sub> (E = Ga, In, and Tl) slightly and the distortion energies are less than 0.02 kcal/mol. The C<sub>2</sub>E<sub>4</sub> (E = Al, Ga, In, and Tl) with dptCs are 18.0, 18.3, 13.4, and 12.2 kcal/mol energetically more favorable than their nearest isomers, respectively, at the CCSD(T)//MP2 level with aug-cc-pVTZ for C and Al and aug-cc-pVTZ-PP for Ga, In, and Tl basis set. The substantial energy differences suggest their promise to be experimentally realized. The strong peak on the C<sub>2</sub>Al<sub>4</sub><sup>-</sup> component in the time-of-flight mass spectrum from laser vaporization of a mixed graphite/aluminum may relate to the *D*<sub>2h</sub> C<sub>2</sub>Al<sub>4</sub> global minimum. The analyses of the electronic structures of C<sub>2</sub>Al<sub>4</sub> (*D*<sub>2h</sub>), CAI<sub>4</sub><sup>2-</sup> (*D*<sub>4h</sub>) and CAI<sub>5</sub><sup>+</sup> (*D*<sub>5h</sub>) indicates that the C<sub>2</sub> moiety in C<sub>2</sub>Al<sub>4</sub> is the equivalence of carbon centers in CAI<sub>4</sub><sup>2-</sup> and CAI<sub>5</sub><sup>+</sup> and unveils the reasons for their stability. The electronic structures of C<sub>2</sub>Al<sub>4</sub> and ethene are compared. On the one hand, an Al atom functions like an H atom because the eight more valence electrons of C<sub>2</sub>Al<sub>4</sub> than C<sub>2</sub>H<sub>4</sub> occupy four nonbonding orbitals and are not effectively utilized for bonding. On the other hand, an Al atom is different from an H atom because an Al atom has p electrons available for peripheral bonding around the C<sub>2</sub> moieties in C<sub>2</sub>Al<sub>4</sub>, which further rationalize the origins for C<sub>2</sub>E<sub>4</sub> to achieve double ptCs.

## 1. Introduction

Linear dicoordination (e.g., ethyne), planar trigonal tricoordination (e.g., ethene) and tetrahedral tetracoordination (e.g., methane) are the predominant bonding patterns of carbon. However, a curious exception, planar tetracoordinate carbon (ptC), has fascinated chemists since the 1970s, when Hoffmann, Alder, and Wilcox<sup>1</sup> suggested ways to reduce the unfavorable energies of ptC disposition after Monkhorst proposed the planar configuration for the interconversion of enantiomers with asymmetric carbon in 1968.<sup>2</sup> Since the first computational prediction of a ptC minimum, 1,1-dilithiocyclopropane, by the Schleyer–Pople group,<sup>3</sup> various molecules with ptCs have been characterized computationally or experimentally.<sup>4–9</sup> Because the coordination number for the conventional planar carbon bonding (e.g., the carbons in ethene and benzene) is three, one can consider planar carbon having a coordination number higher than three, as planar hypercoordinate carbon (phC). Molecules with planar penta- and hexa-coordinate carbon have been computationally predicted to be viable by Wang and Schleyer<sup>10</sup> and Exner and Schleyer,<sup>11</sup> respectively. Recently, the planar

bonding patterns have been further extended to planar hypercoordinate heteroatoms and transition metals.<sup>12–18</sup>

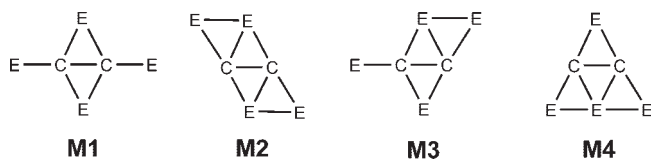
In the phC chemistry, chemists, on one hand, strive to design species containing more and more phCs. For example, the Frenking–Schleyer group<sup>19</sup> recently reported boron rings with multiple phCs. Minyaev et al.<sup>20,21</sup> designed species with several ptCs based on C<sub>3</sub>B<sub>2</sub>H<sub>n</sub> (*n* = 2, 4, and 6) ptC units. Zhang and Cao<sup>22,23</sup> constructed zigzag C–B nanotube with quasi-ptCs. Using the CM<sub>4</sub>H<sub>4</sub> (M = Ni, Pd, Pt) as basic building blocks, Wu et al.<sup>24</sup> designed compounds of various shapes with multiple ptCs or quasi-ptCs. On the other hand, they make efforts to achieve phC in the simplest global minima because being the global minimum can facilitate experimental generations and identifications. For example, the *D*<sub>4h</sub> CAI<sub>4</sub><sup>2-</sup> has been identified to be the simplest penta-atomic global minimum, this species and its analogs, CAI<sub>4</sub><sup>-</sup>,<sup>25</sup> CAI<sub>3</sub>Si<sup>-</sup>,<sup>26</sup> CAI<sub>3</sub>Ge<sup>-</sup>,<sup>26</sup> CAI<sub>4</sub><sup>2-</sup>, and NaCAI<sub>4</sub><sup>-</sup>,<sup>27</sup> have been experimentally detected in 1999 and 2000. Interestingly, their isoelectronic ptC species, *cis*- and *trans*-CAI<sub>2</sub>Si<sub>2</sub>, were predicted by Schleyer and Boldyrev in 1991. However, the effort to detect the phC species CB<sub>7</sub><sup>-</sup> and CB<sub>6</sub><sup>2-</sup> (not global minima)<sup>10,11</sup> led to the more energetically favorable species, in which the carbon atoms prefer locating on the edges or vertexes.<sup>28,29</sup> More examples of simplest global minima with phC, such as CB<sub>4</sub>,<sup>30,31</sup> CAI<sub>5</sub><sup>+</sup>,<sup>32</sup> CCu<sub>4</sub><sup>2+</sup>, and its isoelectronic analogs,<sup>33</sup> have recently been reported. Moreover, the simplest species may be used as the basic building blocks to construct new molecules or materials with multiple phCs. The potential

\* To whom correspondence should be addressed. E-mail: wyb@sxu.edu.cn; zxwang@gucas.ac.cn.

<sup>†</sup> Institute of Molecular Science, the Key Laboratory of Chemical Biology and Molecular Engineering of Education Ministry, Shanxi University.

<sup>‡</sup> College of Chemistry and Chemical Engineering, Graduate University of Chinese Academy of Sciences.

## SCHEME 1: Simplest Models Possibly Containing dptCs



of using small ptC building blocks (e.g.,  $\text{CB}_6^{2-}$ ,<sup>34–39</sup>  $\text{C}_5^{2-}$ ,<sup>40–45</sup>  $\text{CAI}_3\text{Si}$ ,<sup>46</sup> and  $\text{CAI}_4^{2-}$ ,<sup>47</sup>) to design novel materials has been explored theoretically. In this work, we attempted to find the simplest species with double planar tetracoordinate carbons (dptCs), and showed that the obtained  $\text{C}_2\text{E}_4$  (E = Al, Ga, In, and Tl) are not only the simplest species with dptCs, but also the global minima. Note that the “simplest” means the dptC species containing the least number (six) and types (two) of atoms.

## 2. Computational Methods

Scheme 1 sketches the simplest binary models (M1–M4) which possibly contain dptCs. Under the restrictions to these models and to singlet electronic states, we scanned the second- and third-row main group elements at the B3LYP/6–31+G\* level. The species,  $\text{C}_2\text{Al}_4$  (M1) and  $\text{C}_2\text{Be}_4$  (M2), are the only survivors to meet two criteria: minima with dptCs and the DFT wave functions being stable. Other species, such as  $\text{C}_2\text{Li}_4$  (M1 and M2) and  $\text{C}_2\text{Na}_4$  (M2 and M4), are minima with dptCs but their wave functions are unstable.  $\text{C}_2\text{Mg}_4$  has no dptCs minimum under the restrictions. We then extended the scanning to the heavier elements in the group of IIA and IIIA at the B3LYP level with basis sets 6–31+G\* for C, Ca, and Ga and aug-cc-pVDZ-PP<sup>48–50</sup> for In and Tl. At this level,  $\text{C}_2\text{E}_4$  (E = Ga, In, and Tl) are also minima but  $\text{C}_2\text{Ca}_4$  is a first-order saddle point. We therefore discarded  $\text{C}_2\text{E}_4$  (E = Mg and Ca) in the following.

The located species with dptCs were then verified to be global minima using the following procedure. For each  $\text{C}_2\text{E}_4$  (E = Be, Al, Ga, In, and Tl), 3000 random structures were generated by a program called GXYZ,<sup>51</sup> which is principally the same as the “kick” method proposed by Saunders et al.<sup>52,53</sup> Both of the methods generate a large pool of random structures for geometric optimizations. About 80–90% of these random structures were filtered out because they are structurally unreasonable. The remaining 376, 278, 202, 171, and 185 structures for E = Be, Al, Ga, In, and Tl, respectively, were then subjected to optimizations at B3LYP level with the basis

set mentioned above. Ignoring the slight differences due to releasing the symmetry constraint, there were 6, 8, 11, 10, and 12 structures for E = Be, Al, Ga, In, and Tl, respectively, identified to be the same as the dptCs minima optimized on the basis of the models. This implies the good samplings on the potential energy surfaces (PESs). To further examine the sampling convergence, taking  $\text{C}_2\text{Al}_4$  as an example, another independent exploration with 4000 initial random structures was carried out. Optimizations on the 717 initially filtered input structures gave 40 structures having  $D_{2h}$  symmetry with dptCs. In a study on the  $\text{C}_n\text{Al}_m$  ( $n = 2–3$ ,  $m = 2–8$ ) clusters, Naumkin<sup>54</sup> also reported the  $D_{2h}$   $\text{C}_2\text{Al}_4$  species, but it is unclear if it is the global minimum. The dptCs minima, together with the lowest three for  $\text{C}_2\text{E}_4$  (E = Al, Ga, In, and Tl) or five for  $\text{C}_2\text{Be}_4$  isomers obtained in the above step, were then refined and confirmed to be minima by frequency analysis calculations at the B3LYP/aug-cc-pVTZ (aug-cc-pVTZ-PP<sup>48–50</sup> for Ga, In, and Tl) level. Concerning the caveats about the DFT reliability recently raised by several authors,<sup>55–59</sup> the B3LYP geometries (including the dptCs minima) were reoptimized at the MP2/aug-cc-pVTZ (aug-cc-pVTZ-PP for Ga, In, and Tl) level, which resulted in slightly distorted structures for E = Ga, In, Tl (see below). The energetic results were finally improved at the CCSD(T)/aug-cc-pVTZ (aug-cc-pVTZ-PP for Ga, In, and Tl) level using the MP2 structures. The results reported in the following are all calculated with the basis set aug-cc-pVTZ (aug-cc-pVTZ-PP for Ga, In and Tl). The basis set will not be mentioned hereafter, unless otherwise specified. All ab initio and DFT calculations were performed using the *Gaussian 03* program of package.<sup>60</sup> The electronic structures were analyzed by NBO 5.0<sup>61,62</sup> at the B3LYP level.

## 3. Results and Discussion

Being the structures of  $\text{C}_2\text{E}_4$  (E = Al(1a), Ga(2a), In(3a), and Tl(4a)), optimized at the B3LYP and MP2 levels, are shown in Figure 1, and their Cartesian coordinates at the two levels are given in the Supporting Information I (SI1). At the B3LYP level, the  $D_{2h}$  1a–4a are all minima, but at the MP2 level, only  $D_{2h}$  1a is a minimum and  $D_{2h}$  2a, 3a, and 4a are first-order saddle points with very small imaginary frequencies (9i, 16i, and 10i  $\text{cm}^{-1}$ , respectively). Following the vibrational modes corresponding to the imaginary frequencies, the  $D_{2h}$  2a, subjecting to geometrical optimization, degenerated to a planar  $\text{C}_{2v}$  structure with dptCs, but the  $D_{2h}$  3a and 4a to the bending  $\text{C}_{2v}$  structures without perfect ptC (see Figure 1). However, the

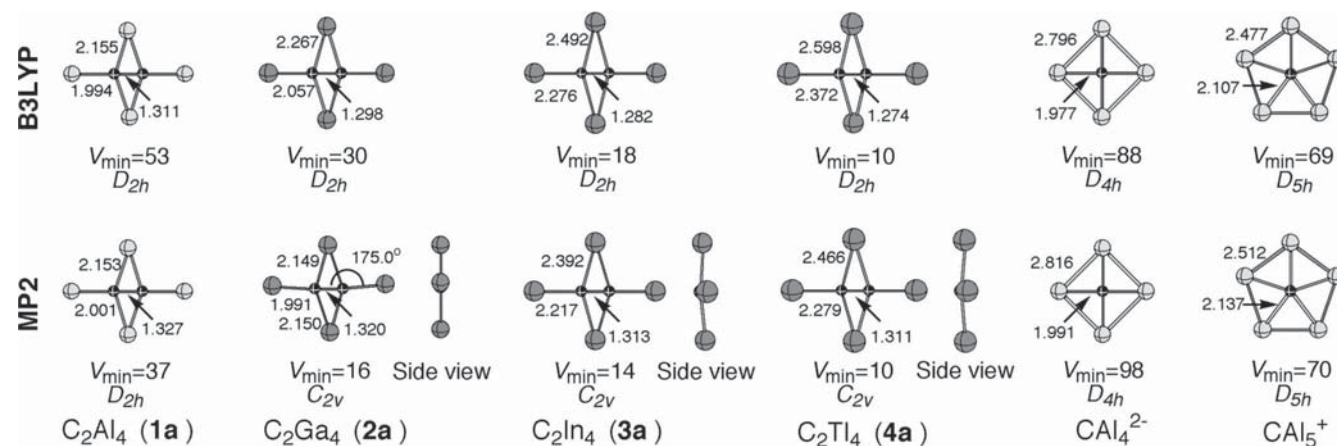


**Figure 1.** B3LYP and MP2 optimized geometries of 1a–4a,  $\text{CAI}_4^{2-}$ , and  $\text{CAI}_5^+$ , together with the numbers of imaginary frequencies (NIMAG) and the lowest vibrational frequencies ( $V_{\min}$ ) in  $\text{cm}^{-1}$ . Bond lengths and bond angles are given in angstroms and degrees, respectively.



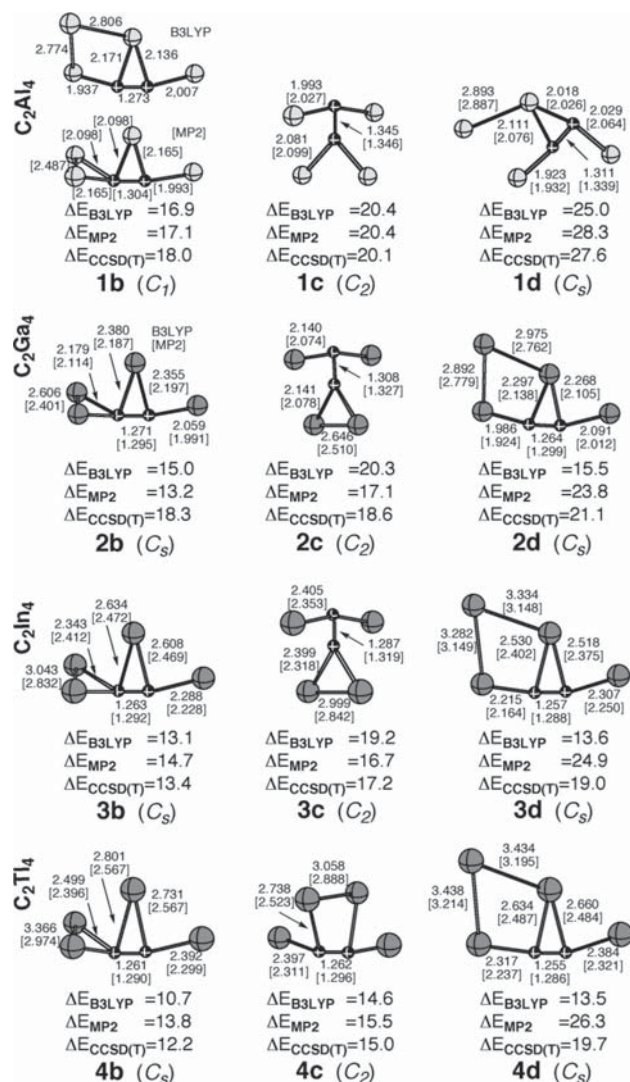


**Figure 2.** B3LYP and MP2 optimized geometries of the three singlet isomers nearest to **1a–4a**, together with the relative energies ( $\Delta E$  in kcal/mol) at the B3LYP, MP2, and CCSD(T)//MP2, respectively. Bond lengths are given in Å. Values in brackets are MP2 results.

energy differences between  $C_{2v}$  and  $D_{2h}$  structures of **2a**, **3a**, and **4a** are very small (less than 0.02 kcal/mol). The negligible differences are much less than the zero point energy corrections and therefore the  $C_{2v}$  **3a** and **4a** can be considered to be fluxionary ptC species and detected as vibrationally averaged planar  $D_{2h}$  structures experimentally.<sup>25,63</sup>

The global minimum is very important for feasibly experimental access, in particular for the laser-ablation-based experiments because the method tends to anneal species into the global minimum.<sup>63</sup> For example, the experimentally detected  $D_{4h}$   $\text{CaAl}_4^-$  and  $\text{CaAl}_4^{2-}$  have been verified to be the global minima computationally.<sup>25,27</sup> However, as mentioned before, the effort to detect the phC species  $\text{CB}_7^-$  and  $\text{CB}_6^{2-}$  (not global minima)<sup>10,11</sup> led to the energetically more favorable species, in which the carbon atoms prefer locating on the edges or vertexes.<sup>28,29</sup> The  $D_{5h}$   $\text{CaI}_5^{+32}$  is also predicted to be the global minimum. Using the procedure described above, we explored the PESs of  $\text{C}_2\text{E}_4$  (E = Al, Ga, In, and Tl) extensively. Figure 2 gives the first three lowest isomers of **1a**, **2a**, **3a**, and **4a**. Although with respect to the symmetry planes containing dptCs, the  $D_{2h}$  structures are fluxional, they are rigid with respect to other freedoms of motions. At the B3LYP level, **1a–4a** are 16.9, 15.0, 13.1, and 10.7 kcal/mol energetically more favorable

than their nearest isomers (**1b–4b**), respectively. The B3LYP relative energies are reasonably in agreement with the MP2 (17.1, 13.2, 14.7, and 13.8 kcal/mol, respectively) and CCSD(T)//MP2 (18.0, 18.3, 13.4, and 12.2 kcal/mol, respectively) values.

We further considered the triplet states of these species and explored their PESs using the same approaches as for the singlet states. Their structural and energetic results are given in SI1, SI4 and SI5. At our highest CCSD(T)//MP2 level, the lowest triplet states of  $\text{C}_2\text{E}_4$  (E = Al, Ga, and In) are 1.6, 2.0, and 0.4 kcal/mol higher in energy than their fourth lowest singlet states, **1d**, **2d**, and **3d**, respectively. The lowest  $\text{C}_2\text{Tl}_4$  triplet state lies between **4c** and **4d** and is 0.1 kcal/mol higher in energy than **4c**. Therefore, we may safely conclude that the singlet species, **1a–4a** shown in Figure 1, are indeed the global minima under the considerations of both singlet and triplet states.

We noted that a time-of-flight mass spectrum from laser vaporization of a mixed graphite/aluminum target, reported by Boldyrev–Wang groups,<sup>63</sup> showed a strong peak on the  $\text{C}_2\text{Al}_4^-$  component, which may relate to the fact that  $\text{C}_2\text{Al}_4$  is the global minimum. We propose further verifications of the species and others reported.

The B3LYP and MP2 optimizations gave the same structures for these isomers except for **1b** (see Figure 2). The first three isomers in the  $\text{C}_2\text{Ga}_4$  (**2b–2d**) and  $\text{C}_2\text{In}_4$  (**3b–3d**) series have similar structures and the same energy order, but **1d** and **4c** have no counterparts in the  $\text{C}_2\text{Ga}_4$  and  $\text{C}_2\text{In}_4$  series. It is remarkable because they are ranked entirely based on the random searches, which implies some common features in their chemical bonding. For all of the four series, the relative energy orders of the isomers, given by MP2 and CCSD(T)//MP2, are identical in spite of their different magnitudes. For  $\text{C}_2\text{Al}_4$  series, the B3LYP order is consistent with those given by MP2 and CCSD(T)//MP2, but the two levels give different orders for  $\text{C}_2\text{Ga}_4$ ,  $\text{C}_2\text{In}_4$ , and  $\text{C}_2\text{Tl}_4$  series and reverse the orders of **c** and **d** isomers. Nevertheless, the three levels unanimously predicted **a** and **b** isomers to be the first two lowest isomers.

The  $C_{2h}$   $\text{C}_2\text{Be}_4$  (**M2**) with dptCs is a local minimum. The exploration on its PES, at the B3LYP/6–31+G\* level, indicates that it is the fifth lowest. The refinement calculations at the B3LYP/aug-cc-pVTZ also rank it the fifth lowest. But the calculations at both MP2 and CCSD(T)//MP2 levels rank it the sixth lowest. At the three levels, the dptC-contained  $\text{C}_2\text{Be}_4$  is 8.8, 11.9, and 9.7 kcal/mol higher in energy than the global minima (**5a**), respectively (see Figure 3, their Cartesian coordinates are given in SI2). It should be mentioned that PES exploration (B3LYP/6–31+G\*) revealed that the global minimum is a planar irregular hexagon. In a recent B3PW91/6–31+G\* study on the  $\text{Be}_n\text{C}_m$  ( $n = 1\sim 10$ ;  $m = 1\sim 11 - n$ , respectively) clusters, Mainardi and co-workers<sup>64</sup> also reported such a hexagonal structure. However, the B3LYP/aug-cc-pVTZ optimization indicates that it is the regular hexagonal global minimum with  $C_{2v}$  symmetry. The MP2 optimizations with aug-cc-pVTZ basis set also led to the  $C_{2v}$  structure but rank it the third lowest. However, the CCSD(T)//MP2 single-point calculations again indicate the  $C_{2v}$  structure to be the global minimum.

Among the twelve vibrational modes of **1a–4a**, only the asymmetric bridging-E( $E_{\text{BR}}$ )–C and terminal-E( $E_{\text{TE}}$ )–C stretching modes show strong activities and the others are entirely inactive or have very small infrared intensities. To aid the experimental identification, Table 1 lists the frequencies and infrared intensities of the two strongest modes of **1a–4a**, along with the strongest modes of  $\text{CaI}_4^{2-}$  and  $\text{CaI}_5^+$ . Although the irreducible representations of C–E stretching vibrational modes at B3LYP and MP2 level for  $\text{C}_2\text{Ga}_4$ ,  $\text{C}_2\text{In}_4$ , and  $\text{C}_2\text{Tl}_4$  are

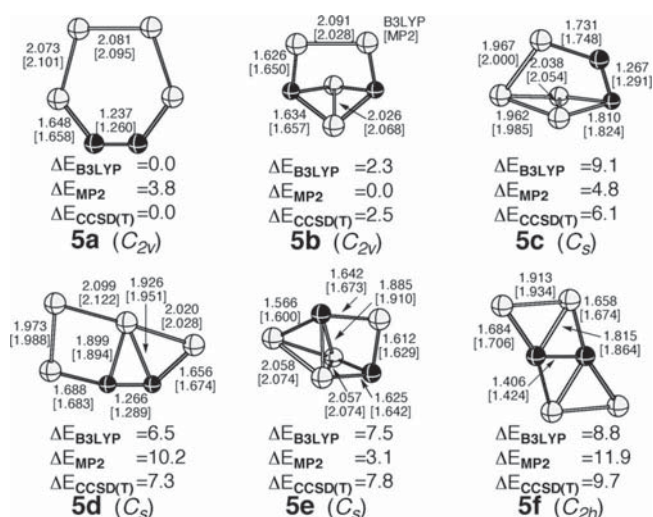
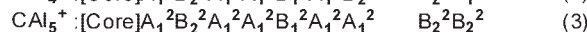
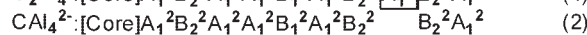
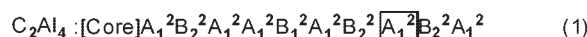


**Figure 3.** B3LYP and MP2 optimized geometries of the six lowest isomers of  $C_2Be_4$ , together with the relative energies ( $\Delta E$  in kcal/mol) and the key bond lengths (in Å). Values in brackets are MP2 results.

different due to their different structures, we have confirmed that the motions of the modes are the same. This holds for  $C_2-E_{BR}$  vibrational modes of the  $C_2Ga_4$  vs  $C_2E_4$  ( $E = In$  and  $Tl$ ) at the MP2 level. Similar to **1a–4a**, the infrared intensities of other modes of  $CaI_4^{2-}$  and  $CaI_5^+$  are much smaller. Therefore, their infrared spectra only have strong peaks on the two modes, which may facilitate experimental identification of these species. As shown in the Table 1, the B3LYP frequency values of **1a–4a** ( $326.8\sim 547.3\text{ cm}^{-1}$  for  $E_{BR}-C$  stretching,  $385.0\sim 602.4\text{ cm}^{-1}$  for  $E_{TE}-C$  stretching) are in agreement with those of MP2 values. The decreasing vibrational frequencies from **1a** to **4a** indicate the weakening C–E bonding as E moves down the periodical table. Note that the vibration frequencies of  $Al_{TE}-C$  and  $Al_{BR}-C$  stretching in **1a**,  $602.4$  and  $547.3\text{ cm}^{-1}$ , respectively, are comparable to the Al–C stretching at  $736.1\text{ cm}^{-1}$  for  $CaI_4^{2-}$  and  $631.9\text{ cm}^{-1}$  for  $CaI_5^+$ , respectively. Consistently, the  $Al_{TE}-C$  and  $Al_{BR}-C$  bond lengths,  $1.994$  and  $2.155\text{ Å}$ , respectively are compared with the  $1.977$  in  $CaI_4^{2-}$  and  $2.107\text{ Å}$  in  $CaI_5^+$ .

$CaI_4^{2-}$  and  $CaI_5^+$  are isoelectronic and have been characterized to be the global minima.<sup>27,32</sup> In their common  $C_{2v}$  subgroup,  $CaI_4^{2-}$  and  $CaI_5^+$  have the same electron configurations except for the orders of the three highest occupied molecular orbitals (MOs) (eqs 2 and 3).  $C_2Al_4$  has two electrons more than  $CaI_4^{2-}$  and  $CaI_5^+$  and the two extra electrons occupy HOMO-2 (framed in eq 1) which is absent in  $CaI_4^{2-}$  and  $CaI_5^+$ . Except for this orbital, the occupied MOs of **1a** have the same symmetries (orbital shapes) as those of  $CaI_4^{2-}$  and  $CaI_5^+$  (eqs 1–3 and Figure 4). The HOMO of  $CaI_4^{2-}$  and the HOMO-2 of  $CaI_5^+$ ,

which were proposed to contribute to stabilizing their pTC arrangements, have a counterpart in **1a** (i.e., the HOMO). Note that a similar orbital is also present in the boraplanes designed by Wang and Schleyer.<sup>65</sup> The Wiberg bond indices (WBIs) and the NBO charges given by NBO analyses are summarized in Table 2. Although **1a**,  $CaI_4^{2-}$ , and  $CaI_5^+$  are in the different charge states, the  $C_2$  moiety in **1a** bears charges ( $-2.78e$ ), close to those of the carbon centers in  $CaI_4^{2-}$  ( $-2.72e$ ) and  $CaI_5^+$  ( $-2.80e$ ), which, along with their similarities in MO shapes (see Figure 4), suggests that the  $C_2$  moiety in **1a** can be viewed as the equivalences of the carbon centers in  $CaI_4^{2-}$  and  $CaI_5^+$ . If the  $C_2$  moiety in **1a** are viewed as an unit to interact with the peripheral  $Al_4$  ring, then its total WBI of the moiety,  $2.02 [(3.11-2.10) \times 2]$ , to the  $Al_4$  periphery is comparable to those,  $2.24$  in  $CaI_4^{2-}$  and  $2.15$  in  $CaI_5^+$ . This further rationalizes our deduction. Recall that the C–Al stretching vibrational modes in **1a**,  $CaI_4^{2-}$ , and  $CaI_5^+$  all are most strongly active while other modes are inactive or have negligible infrared intensities. Therefore, the bonding interactions between the  $C_2$  moiety and the  $Al_4$  periphery in **1a** are similar to those between C and  $Al_4$  or  $Al_5$  periphery in  $CaI_4^{2-}$  and  $CaI_5^+$ , respectively. Indeed, the WBIs of  $Al_{BR}-$  and  $Al_{TE}-C_2$  moiety in **1a**,  $0.51$  and  $0.56$ , respectively, are comparable to the  $0.56$  in  $CaI_4^{2-}$  and  $0.43$  in  $CaI_5^+$  (Table 2). Due to their different charge states, the electrostatic interactions between the centers and the  $Al_4$  (or  $Al_5$ ) periphery vary, as reflected by the NBO charges on the Al atoms. However, the Al–Al bonding in **1a** are different from those in  $CaI_4^{2-}$  and  $CaI_5^+$ . The sum of WBIs of  $Al_{BR}-Al$  ( $0.29$ ) and  $Al_{TE}-Al$  ( $0.22$ ) are significantly smaller than the  $1.34$  in  $CaI_4^{2-}$  and  $1.39$  in  $CaI_5^+$ . Among the occupied MOs, one can identify that the major contributions to the differences come from HOMO-6 of **1a**. This MO in **1a** is involved in C– $Al_{TE}$  and C–C  $\sigma$  bonding, whereas the corresponding orbital (HOMO-5) in  $CaI_4^{2-}$  and  $CaI_5^+$  contribute to the  $\sigma$  Al peripheral bonding. Because **1a** is neutral, the charges on the  $C_2$  moiety are donated by the peripheral Al atoms, the  $Al_{BR}$  and  $Al_{TE}$  bear  $0.69e$  and  $0.70e$  positive charges, respectively. In contrast, the Al atoms in  $CaI_4^{2-}$  have a much smaller positive charge ( $0.18e$ ), which is due to the net negative  $2e$  charges of the dianion. Although  $CaI_5^+$  possesses  $1e$  positive charge, the Al atoms in  $CaI_5^+$  have  $0.76e$  positive charges, comparable to those in **1a**. This is because the extra Al atom in  $CaI_5^+$  compensates the effects of the monocationic charge state of  $CaI_5^+$ .



The natural electron configurations of Al atoms in **1a**,  $CaI_4^{2-}$ , and  $CaI_5^+$  are compared in Table 3. Similar to  $CaI_4^{2-}$  and

**TABLE 1: Wavenumbers (WN, in  $\text{cm}^{-1}$ ) of the Most Active C–E Stretching Modes with Their Symmetries (SYM) and Intensities (Int, in  $\text{km/mol}$ ) of **1a–4a**,  $CaI_4^{2-}$  and  $CaI_5^+$ , Calculated at B3LYP and MP2 (in parentheses) Levels<sup>a</sup>**

	$E_{TE}-C$ stretching			$E_{BR}-C$ stretching		
	SYM	WN	Int	SYM	WN	Int
$C_2Al_4$ ( <b>1a</b> )	$B_{1u}$ ( $B_{1u}$ )	602.4 (615.9)	635.2 (626.7)	$B_{2u}$ ( $B_{2u}$ )	547.3 (571.6)	372.3 (366.9)
$C_2Ga_4$ ( <b>2a</b> )	$B_{1u}$ ( $B_2$ )	499.0 (581.2)	527.8 (617.0)	$B_{2u}$ ( $A_1$ )	423.7 (539.0)	252.3 (319.2)
$C_2In_4$ ( <b>3a</b> )	$B_{1u}$ ( $B_2$ )	422.4 (497.2)	352.9 (450.7)	$B_{2u}$ ( $B_1$ )	370.6 (458.1)	172.9 (256.3)
$C_2Tl_4$ ( <b>4a</b> )	$B_{1u}$ ( $B_2$ )	385.0 (468.8)	229.4 (397.5)	$B_{2u}$ ( $B_1$ )	326.8 (439.3)	93.4 (210.2)
$CaI_4^{2-}$	$E_u$ ( $E_u$ )	736.1 (785.2)	652.1 (866.6)			
$CaI_5^+$	$E_1'$ ( $E_1'$ )	631.9 (626.5)	380.0 (344.9)			

<sup>a</sup> Note that the C–Al stretching modes of  $CaI_4^{2-}$  and  $CaI_5^+$  are degenerated.



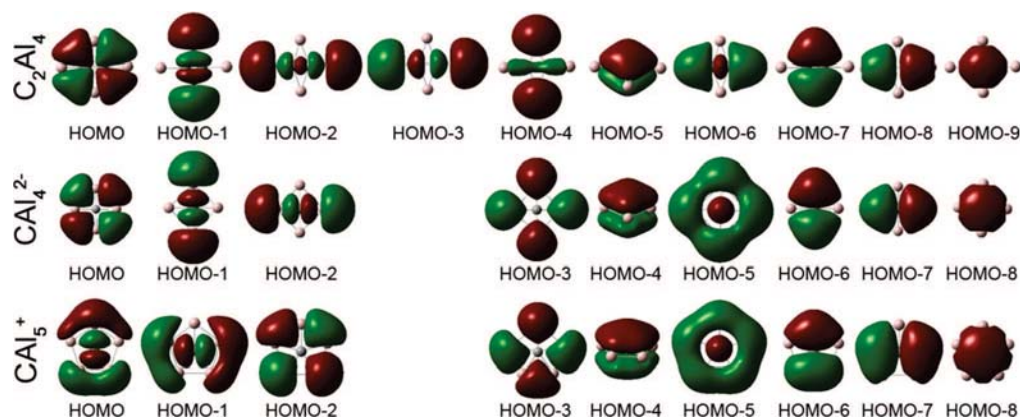


Figure 4. Comparisons of the occupied valence MOs of **1a** with those of  $\text{CAI}_4^{2-}$  and  $\text{CAI}_5^+$ .

TABLE 2: NBO Charges (in  $e$ ) and Wiberg Bond Indices (WBI) of **1a–4a**,  $\text{CAI}_4^{2-}$ , and  $\text{CAI}_5^+$

	$q_C$	$q_E$		$\text{WBI}_C$	$\text{WBI}_E$		$\text{WBI}_{C-C}$	$\text{WBI}_{E-CC}$		$\text{WBI}_{E-Es}$	
		$E_{BR}$	$E_{TE}$		$E_{BR}$	$E_{TE}$		$E_{BR}$	$E_{TE}$	$E_{BR}$	$E_{TE}$
$\text{C}_2\text{Al}_4$ ( <b>1a</b> )	-1.39	+0.69	+0.70	3.11	0.80	0.72	2.10	0.51	0.50	0.29	0.22
$\text{C}_2\text{Ga}_4$ ( <b>2a</b> )	-1.19	+0.59	+0.60	3.30	0.86	0.83	2.17	0.57	0.54	0.32	0.25
$\text{C}_2\text{In}_4$ ( <b>3a</b> )	-1.11	+0.55	+0.56	3.36	0.90	0.89	2.35	0.48	0.54	0.42	0.35
$\text{C}_2\text{Tl}_4$ ( <b>4a</b> )	-1.01	+0.50	+0.51	3.42	0.93	0.95	2.44	0.45	0.53	0.48	0.42
$\text{C}_2\text{B}_4$	-1.02	+0.45	+0.57	3.43	1.31	0.90	1.74	0.95	0.73	0.36	0.16
$\text{CAI}_4^{2-}$	-2.72		+0.18	2.24		1.90			0.56		1.34
$\text{CAI}_5^+$	-2.80		+0.76	2.14		1.99			0.43		1.56
$\text{C}_2\text{H}_4$	-0.37		+0.18	3.94		0.81	2.05		0.95		0.02

TABLE 3: Natural Electron Configurations of E Atoms in **1a–4a**,  $\text{CAI}_4^{2-}$ , and  $\text{CAI}_5^+$

		s	$p_x$	$p_y$	$p_z$
<b>1a</b>	$\text{Al}_{TE}$	1.83	0.26	0.19	0.01
	$\text{Al}_{BR}$	1.83	0.24	0.22	0.01
<b>2a</b>	$\text{Ga}_{TE}$	1.88	0.27	0.24	0.01
	$\text{Ga}_{BR}$	1.90	0.30	0.19	0.02
<b>3a</b>	$\text{In}_{TE}$	1.90	0.23	0.34	0.01
	$\text{In}_{BR}$	1.92	0.35	0.35	0.01
<b>4a</b>	$\text{Tl}_{TE}$	1.93	0.22	0.34	0.01
	$\text{Tl}_{BR}$	1.95	0.39	0.15	0.01
$\text{CAI}_4^{2-}$		1.53	0.61	0.56	0.10
$\text{CAI}_5^+$		1.45	0.38	0.30	0.09

$\text{CAI}_5^+$ , the Al  $3p_z$  orbital in **1a** has very small occupancy,  $0.01e$ , in comparison with  $0.10e$  ( $\text{CAI}_4^{2-}$ ) and  $0.09e$  ( $\text{CAI}_5^+$ ). Because  $\text{CAI}_4^{2-}$  is  $2e$  negatively charged, its  $\sigma$  electron ( $3p_x + 3p_y$ ) occupancy ( $1.17e$ ) of Al atom is larger than the  $0.68e$  in  $\text{CAI}_5^+$  and  $0.45e$  of  $\text{Al}_{TE}/0.46e$  of  $\text{Al}_{BR}$ . The natural electron configuration points out that Al ligands mainly serve as  $\sigma$  electron donors in the three species. Previously, on the basis of the electronic structures of planar methane, Hoffmann, Alder, and Wilcox<sup>1</sup> suggested using  $\sigma$ -donor/ $\pi$ -acceptor ligands to enhance the electronic deficient  $\sigma$  bonding between ptC and ligands and delocalize the unfavorable lone pair on ptC of planar methane. However,  $\text{CAI}_4^{2-}$  and  $\text{CAI}_5^+$  have MOs similar to the lone pair in the planar methane. Note that there are  $\pi$  interactions between ptC and peripheral Al atoms, but the interactions are small (see HOMO-4 in Figure 4). We<sup>66</sup> have rationalized the phenomena in the  $\text{C}(\text{BeH})_4^{2-}$  system, and partially attributed to the weakening effects on the rigidity of the tetrahedral carbon, exerted by the metallic ligands. In contrast, **1a** has no such  $\pi$  lone-pair but a C–C  $\pi$  bonding orbital (HOMO-5) predominantly located on the  $\text{C}_2$  moiety. One may ask that the Al–Al bonding in  $\text{CAI}_4^{2-}$  and  $\text{CAI}_5^+$  is much stronger than that in **1a**, why **1a** still can achieve the planarity? The answer is that the energetic benefit due to the C–C  $\pi$  bonding in **1a** compensate the energetic favorable  $\text{Al}_4$  (or  $\text{Al}_5$ )  $\sigma$  peripheral bonding

(HOMO-5) in  $\text{CAI}_4^{2-}$  and  $\text{CAI}_5^+$ , which are supported by the relatively larger  $\text{WBI}_C$  (3.11 vs. 2.24 and 2.14) and smaller  $\text{WBI}_{\text{Al-Als}}$  (less than 0.3 vs. 1.34 and 1.56) in **1a** than those in  $\text{CAI}_4^{2-}$  and  $\text{CAI}_5^+$ .

The above analyses have revealed that the  $\text{C}_2$  moiety in **1a** can be considered as the equivalence of carbon center in  $\text{CAI}_4^{2-}$  and  $\text{CAI}_5^+$ . How feasible can another carbon be embedded into the  $\text{Al}_4$  ring? If considering **1a** as the product of  $\text{CAI}_4$  ( $T_d$ , the global minimum<sup>67</sup>) + C ( $^3P$ ) reaction, the reaction enthalpies ( $\Delta H^\theta$ ) are  $-156.9$ ,  $-163.8$ ,  $-185.0$  kcal/mol at the B3LYP, MP2, and CCSD(T)//MP2 levels, respectively, indicating the high energetic favorableness of incorporating a C atom into  $T_d$   $\text{CAI}_4$ .

Summarizing the above comparisons, one can concisely understand the stabilities of these species as illustrated by Figure 5. For  $\text{CAI}_4^{2-}$ , addition of the two electrons in  $T_d$   $\text{CAI}_4$  results in the ptC global minimum, because the two extra electrons take the advantage of the peripheral bonding MO<sup>27</sup> (a useful orbital not being utilized in neutral  $D_{4h}$   $\text{CAI}_4$ , which is the third-order saddle point). The two electrons in  $\text{CAI}_5^+$  are introduced by adding an  $\text{Al}^+$  in the  $\text{Al}_4$  ring. In **1a**, the addition of two electrons is fulfilled by introducing another carbon in the center. Although the carbon brings four electrons, two of them are used for an internal C–C bonding. The neutrality of **1a** may facilitate

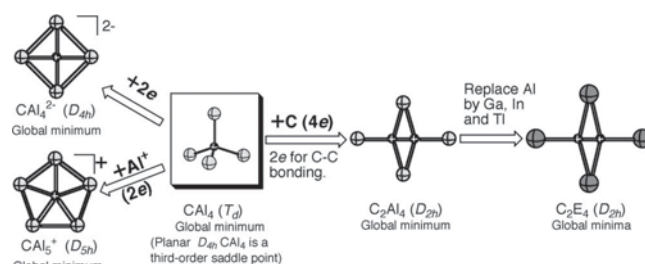
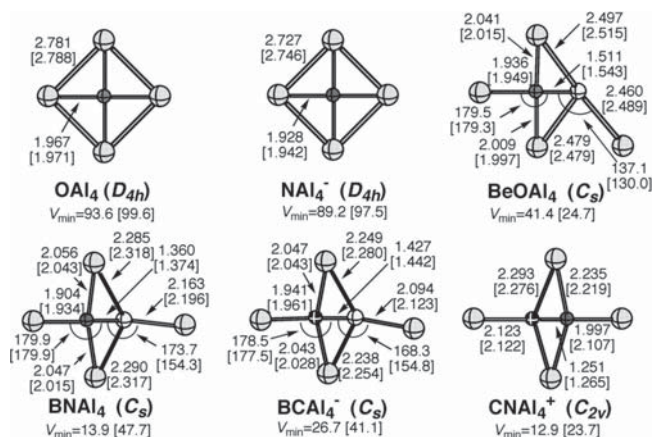


Figure 5. Relationships of  $\text{CAI}_4$ ,  $\text{CAI}_4^{2-}$ ,  $\text{CAI}_5^+$ , and  $\text{C}_2\text{Al}_4$ .



**Figure 6.** B3LYP and MP2 optimized geometries of OAl<sub>4</sub>, NAl<sub>4</sub><sup>-</sup>, BeOAl<sub>4</sub>, BNAl<sub>4</sub>, CNAl<sub>4</sub><sup>+</sup>, and BCAl<sub>4</sub><sup>-</sup>, together with the smallest harmonic frequencies ( $V_{\min}$  in  $\text{cm}^{-1}$ ) and the geometrical parameters (the bond lengths in Å and bond angles in degree). The values in bracket are the MP2 results.

generation and detection in the experiments (e.g., low temperature matrix isolation).

The established equivalence relationship can be used to design more molecules with planar tetracoordinate heteroatoms (Figure 6, the Cartesian coordinates are given in the SI3). The previously reported OAl<sub>4</sub> and NAl<sub>4</sub><sup>-</sup> are reconfirmed to be minima in the present levels of theories. Similarly, at both B3LYP and MP2 levels, the replacements of C<sub>2</sub> moiety in C<sub>2</sub>Al<sub>4</sub> by the isoelectronic BeO, BN, BC<sup>-</sup>, and CN<sup>+</sup> moieties also lead to minima, BeOAl<sub>4</sub>, BNAl<sub>4</sub>, BCAl<sub>4</sub><sup>-</sup>, and CNAl<sub>4</sub><sup>+</sup>. Due to the stronger metallic characters and bigger radius of Be and B than C, the terminal Al atoms bonded to Be or B in BeOAl<sub>4</sub> and BNAl<sub>4</sub> and BCAl<sub>4</sub><sup>-</sup> bend away from the BeO or BC axes. Consistently, the bending Al atom in BeOAl<sub>4</sub> is further away from the BeO axis than the Al atoms in BNAl<sub>4</sub> and BCAl<sub>4</sub><sup>-</sup> from BN and BC axis. The terminal Al atoms in CNAl<sub>4</sub><sup>+</sup> lie along the CN axis.

The C–C double bonding ( $\text{WBI}_{\text{C}=\text{C}} = 2.11$ ) and *D*<sub>2h</sub> symmetry of **1a** reminds us of the classical ethene. As reflected by the WBIs and NBO charges (Table 2), the replacement of hydrogens in ethene by alumina results in the common differences expected on the basis of the fact that Al is more metallic than H. The MO analyses give more insights. As compared in the Figure 7, the eight more valence electrons in **1a** than in C<sub>2</sub>H<sub>4</sub> can be assigned to the HOMO-4 to HOMO-1 MOs (right column), which can be considered as nonbonding MOs. Note that CAL<sub>4</sub><sup>2-</sup> and CAL<sub>4</sub><sup>+</sup> also have four occupied nonbonding MOs (including the HOMO-5, see Figure 4). Interestingly, although Al has two more valence electrons available than hydrogen, they are not efficiently utilized for bonding interactions and occupy the nonbonding orbitals (i.e., the HOMO-1~HOMO-4 of C<sub>2</sub>Al<sub>4</sub>, as shown in Figure 7) in these species. The pair of HOMO-9 and HOMO-8 in **1a** corresponds to the pair of HOMO-5 and HOMO-4 in C<sub>2</sub>H<sub>4</sub>, which originates from the bonding and antibonding interactions between two carbon 2s orbitals. The  $\pi$  (HOMO-5) and  $\sigma$  (HOMO-6) MOs in **1a** have counterparts in ethene, HOMO and HOMO-2, respectively. The essential differences lie in the HOMO and HOMO-7 of **1a**. On the basis of the consideration of orbital symmetry, the two MOs of **1a** correspond to HOMO-1 and HOMO-3 of ethene, respectively. The ethene HOMO-1 contributes to the C–H  $\sigma$  bonding and has negative contribution to the C–C bonding, whereas the corresponding orbital (HOMO) of **1a** contributes to the peripheral Al<sub>4</sub> bonding and the antibonding interaction between carbons is negligible, which reflects the differences between

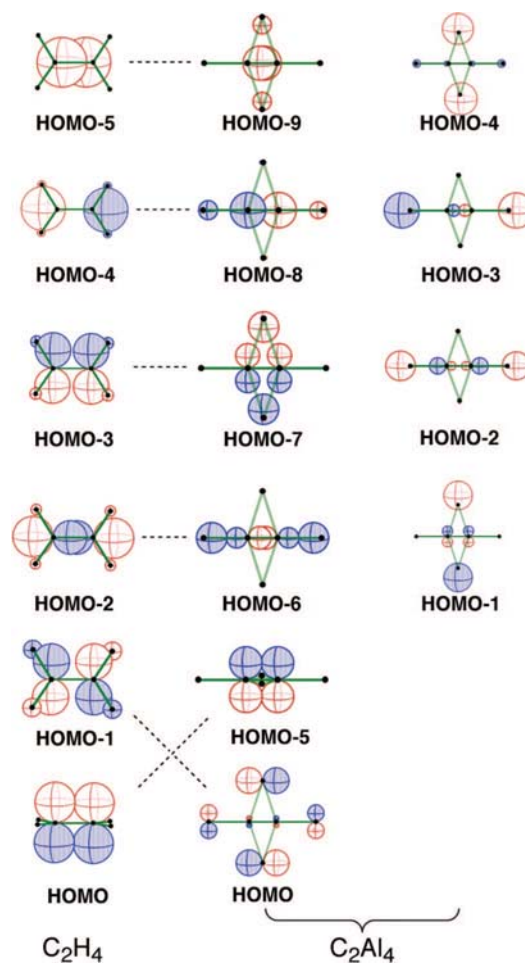


**Figure 7.** Comparison of the valence MOs of **1a** with those of ethylene.

Al and H atoms, that is, Al has p electrons available for such covalent bonding. The ethene HOMO-3 contribute to the four C–H bonds and C–C bonding, in contrast, the electrons in HOMO-7 of **1a** bound two of the Al atoms in the bridging positions. This can be attributed to the electron deficiency of the Al atom, similar to the bridging hydrogens in carbocations.

The MOs of **1a**, **2a**, **3a**, and **4a**, given in SI6, indicate the similarities in their electronic structures, although the MO energy order may vary. However, the individual characters of the ligands results in differences in their bonding as quantified by WBI and NBO charges. As the E atoms move down the periodical table (from Al to Tl), because their electronegativities (1.5(Al), 1.6(Ga), 1.7(In), 1.8(Tl))<sup>68</sup> increase, the NBO charges on the C<sub>2</sub> moieties,  $-2.78$ ,  $-2.38$ ,  $-2.22$ , and  $-2.02e$  for **1a–4a**, respectively, decrease gradually. The decreasing C–C bond lengths, 1.311, 1.298, 1.282, and 1.274 Å in **1a–4a**, respectively, are consistent with the increasing  $\text{WBI}_{\text{C}=\text{C}}$ , 2.10(**1a**), 2.17 (**2a**), 2.35 (**3a**), and 2.44 (**4a**), respectively.

Boron is the only exception for Group IIIA elements to form *D*<sub>2h</sub> C<sub>2</sub>B<sub>4</sub> species with dptCs. Zeng et al.<sup>31</sup> have explored the PES of C<sub>2</sub>B<sub>4</sub>. Our calculations at the B3LYP/aug-cc-pVTZ level showed the *D*<sub>2h</sub> C<sub>2</sub>B<sub>4</sub> with dptCs is a forth-order saddle point and 187.3 kcal/mol higher in energy than the reported global minimum,<sup>31</sup> in which two carbons bond to a B<sub>4</sub> ring externally. We reason as follows: As discussed in our C(BeH)<sub>4</sub><sup>2-</sup> paper,<sup>66</sup> the rigidity of a tetrahedral carbon become weaker as the ptC-ligand bonds become less covalent. The average WBI of C–B bonds in the *D*<sub>2h</sub> C<sub>2</sub>B<sub>4</sub>, 0.84, is substantially larger than the average WBIs (0.51, 0.56, 0.51, and 0.49) in **1a–4a**, respec-



tively. Although  $D_{2h}$   $C_2B_4$  also possesses a  $B_4$  peripheral occupied MOs similar to HOMO and HOMO-5 of  $C_2Al_4$ , the  $B_4$  ring is too small to accommodate two carbons. Note that the  $D_{4h}$   $CB_4^{2-}$  is even not a minimum (it is a second-order saddle point).

### 3. Conclusions

Using ab initio and DFT calculations, we have searched for the smallest species with dptCs. The scanning on the candidates,  $C_2E_4$  ( $E$  = the second- and third-row main group elements) resulted in three minima ( $C_2E_4$  ( $E$  = Be, Mg, and Al)). The DFT PES exploration shows the  $C_2E_4$  ( $E$  = Al–Tl) not only has structures with dptCs but are also global minima. At the CCSD(T)//MP2 level, they are confirmed again to be the global minima, and locate 18.0, 18.3, 13.4, and 12.2 kcal/mol lower than their nearest isomers, respectively.  $C_2Be_4$  is a local minimum. The comparisons of  $D_{2h}$   $C_2Al_4$  with  $CAI_4^{2-}$  and  $CAI_5^+$  uncover that the  $C_2$  moiety in the former is the equivalence of the carbon centers in the later. Concisely, the stabilities of these species can be rationalized as follow: The addition of two electrons in  $CAI_4$  (i.e.,  $CAI_4^{2-}$ ) can utilize a  $Al_4$  peripheral bonding MO.  $CAI_5^+$  obtains the two electrons by incorporating an  $Al^+$  atom in the ring. The addition of two electrons in  $C_2Al_4$  (and its analogs) is fulfilled by incorporating a carbon in the center of  $CAI_4$ . Although the carbon brings four electrons, two of them are utilized for an internal C–C bonding. Although DFT calculations characterized **1a–4a** to have  $D_{2h}$  structures with perfect dptCs, the MP2 optimizations distorted the  $D_{2h}$  symmetry slightly. The energy differences between  $D_{2h}$  and the distorted structures are marginal (<0.02 kcal/mol). The MO comparisons of **1a** with ethene further rationalized the origins of **1a–4a** to achieve dptCs.

**Acknowledgment.** We dedicate the work to Professor Pin Yang on the occasion of his 75th birthday. The authors thank the Shanxi University, the Chinese Academy of Sciences and NSFC (20773160 to Z.X.W. and 20573088 to S.D.L.) for funding. The authors appreciate Prof. Yue-Kui Wang and Dr. Cai-Xia Yuan for their valuable discussions.

**Supporting Information Available:** The Cartesian coordinates and total energies of **1a–4a** and their three singlet isomers, three triplet isomers, the  $C_2Be_4$  isomers and the  $OAl_4$ ,  $NAI_4^-$ ,  $BeOAl_4$ ,  $BNAI_4$ ,  $BCAI_4^-$ , and  $CNAI_4^+$ , the pictures and relative energies of triplet isomers for **1a–4a**, the pictures of occupied valence MOs of **1a–4a** and  $C_2B_4$ , and the complete ref 60. This material is available free of charge via the Internet at <http://pubs.acs.org>.

### References and Notes

- Hoffmann, R.; Alder, R. W.; Wilcox, C. F., Jr. *J. Am. Chem. Soc.* **1970**, *92*, 4992.
- Monkhorst, H. *J. Chem. Commun.* **1968**, 1111.
- Collins, J. B.; Dill, J. D.; Jemmis, E. D.; Apeloig, Y.; Schleyer, P. v. R.; Seeger, R.; Pople, J. A. *J. Am. Chem. Soc.* **1976**, *98*, 5419.
- Keese, R. *Chem. Rev.* **2006**, *106*, 4787, and references therein.
- Merino, G.; Mendez-Rojas, M. A.; Vela, A.; Heine, T. *J. Comput. Chem.* **2007**, *28*, 362, and references therein.
- Siebert, W.; Gunale, A. *Chem. Soc. Rev.* **1999**, *28*, 367, and references therein.
- Sorger, K.; Schleyer, P. v. R. *J. Mol. Struct.: Theochem.* **1995**, *338*, 317, and references therein.
- Rottger, D.; Erker, G. *Angew. Chem., Int. Ed. Engl.* **1997**, *36*, 813, and references therein.
- Radom, L.; Rasmussen, D. R. *Pure Appl. Chem.* **1998**, *70*, 1977, and references therein.
- Wang, Z. X.; Schleyer, P. v. R. *Science* **2001**, *292*, 2465.
- Exner, K.; Schleyer, P. v. R. *Science* **2000**, *290*, 1937.

- Islas, R.; Heine, T.; Ito, K.; Schleyer, P. v. R.; Merino, G. *J. Am. Chem. Soc.* **2007**, *129*, 14767.
- Li, S. D.; Ren, G. M.; Miao, C. Q.; Jin, Z. H. *Angew. Chem., Int. Ed.* **2004**, *43*, 1371.
- Lein, M.; Frunzke, J.; Frenking, G. *Angew. Chem., Int. Ed.* **2003**, *42*, 1303.
- Li, S. D.; Miao, C. Q. *J. Phys. Chem. A* **2005**, *109*, 7594.
- Li, S. D.; Ren, G. M.; Miao, C. Q. *Inorg. Chem.* **2004**, *43*, 6331.
- Luo, Q. *Sci. Chin., Ser. B: Chem.* **2008**, *51*, 607.
- Averkiev, B. B.; Boldyrev, A. I. *Russ. J. Gen. Chem.* **2008**, *78*, 769.
- Erhardt, S.; Frenking, G.; Chen, Z. F.; Schleyer, P. v. R. *Angew. Chem., Int. Ed.* **2005**, *44*, 1078.
- Minyaev, R. M.; Avakyan, V. E.; Starikov, A. G.; Gribanova, T. N.; Minkin, V. I. *Dokl. Chem.* **2008**, *419*, 101.
- Minyaev, R. M.; Gribanova, T. N.; Minkin, V. I.; Starikov, A. G.; Hoffmann, R. *J. Org. Chem.* **2005**, *70*, 6693.
- Sun, W. X.; Zhang, C. J.; Cao, Z. X. *J. Phys. Chem. C* **2008**, *112*, 351.
- Zhang, C. J.; Sun, W. X.; Cao, Z. X. *J. Am. Chem. Soc.* **2008**, *130*, 5638.
- Wu, Y. B.; Yuan, C. X.; Gao, F.; Lu, H. G.; Guo, J. C.; Li, S. D.; Wang, Y. K.; Yang, P. *Organometallics* **2007**, *26*, 4395.
- Li, X.; Wang, L. S.; Boldyrev, A. I.; Simons, J. *J. Am. Chem. Soc.* **1999**, *121*, 6033.
- Wang, L. S.; Boldyrev, A. I.; Li, X.; Simons, J. *J. Am. Chem. Soc.* **2000**, *122*, 7681.
- Li, X.; Zhang, H. F.; Wang, L. S.; Geske, G. D.; Boldyrev, A. I. *Angew. Chem., Int. Ed.* **2000**, *39*, 3630.
- Wang, L. M.; Huang, W.; Averkiev, B. B.; Boldyrev, A. I.; Wang, L. S. *Angew. Chem., Int. Ed.* **2007**, *46*, 4550.
- Averkiev, B. B.; Zubarev, D. Y.; Wang, L. M.; Huang, W.; Wang, L. S.; Boldyrev, A. I. *J. Am. Chem. Soc.* **2008**, *130*, 9248.
- Sateesh, B.; Reddy, A. S.; Sastry, G. N. *J. Comput. Chem.* **2007**, *28*, 335.
- Pei, Y.; Zeng, X. C. *J. Am. Chem. Soc.* **2008**, *130*, 2580.
- Pei, Y.; An, W.; Ito, K.; Schleyer, P. v. R.; Zeng, X. C. *J. Am. Chem. Soc.* **2008**, *130*, 10394.
- Roy, D.; Corminboeuf, C.; Wannere, C. S.; King, R. B.; Schleyer, P. v. R. *Inorg. Chem.* **2006**, *45*, 8902.
- Li, S. D.; Guo, J. C.; Miao, C. Q.; Ren, G. M. *Angew. Chem., Int. Ed.* **2005**, *44*, 2158.
- Li, S. D.; Miao, C. Q.; Ren, G. M.; Guo, J. C. *Eur. J. Inorg. Chem.* **2006**, 2567.
- Ito, K.; Chen, Z. F.; Corminboeuf, C.; Wannere, C. S.; Zhang, X. H.; Li, Q. S.; Schleyer, P. v. R. *J. Am. Chem. Soc.* **2007**, *129*, 1510.
- Luo, Q.; Zhang, X. H.; Huang, K. L.; Liu, S. Q.; Yu, Z. H.; Li, Q. S. *J. Phys. Chem. A* **2007**, *111*, 2930.
- Li, S. D.; Miao, C. Q.; Guo, J. C. *J. Phys. Chem. A* **2007**, *111*, 12069.
- Shahbazian, S.; Alizadeh, S. *J. Phys. Chem. A* **2008**, *112*, 10365.
- Merino, G.; Mendez-Rojas, M. A.; Vela, A. *J. Am. Chem. Soc.* **2003**, *125*, 6026.
- Merino, G.; Mendez-Rojas, M. A.; Beltraan, H. I.; Corminboeuf, C.; Heine, T.; Vela, A. *J. Am. Chem. Soc.* **2004**, *126*, 16160.
- Pancharatna, P. D.; Mendez-Rojas, M. A.; Merino, G.; Vela, A.; Hoffmann, R. *J. Am. Chem. Soc.* **2004**, *126*, 15309.
- Perez, N.; Heine, T.; Barthel, R.; Seifert, G.; Vela, A.; Mendez-Rojas, M. A.; Merino, G. *Org. Lett.* **2005**, *7*, 1509.
- Perez-Peralta, N.; Sanchez, M.; Martin-Polo, J.; Islas, R.; Vela, A.; Merino, G. *J. Org. Chem.* **2008**, *73*, 7037.
- Esteves, P. M.; Ferreira, N. B. P.; Corroa, R. J. *J. Am. Chem. Soc.* **2005**, *127*, 8680.
- Yang, L. M.; Ding, Y. H.; Sun, C. C. *J. Am. Chem. Soc.* **2007**, *129*, 1900.
- Yang, L. M.; Ding, Y. H.; Sun, C. C. *J. Am. Chem. Soc.* **2007**, *129*, 658.
- Peterson, K. A. *J. Chem. Phys.* **2003**, *119*, 11099.
- Schuchardt, K. L.; Didier, B. T.; Elsethagen, T.; Sun, L. S.; Gurumoorhi, V.; Chase, J.; Li, J.; Windus, T. L. *J. Chem. Inf. Model.* **2007**, *47*, 1045.
- Feller, D. *J. Comput. Chem.* **1996**, *17*, 1571.
- Lu, H.-G. In *GXYZ Ver. 1.0, A Random Cartesian Coordinates Generating Program*; Shanxi University: Taiyuan, 2008. We also examined the method by exploring the PESSs of  $CCu_4^{2+}$  and  $CAI_5^+$  and the same global minima were found as reported.
- Saunders, M. J. *J. Comput. Chem.* **2004**, *25*, 621.
- Bera, P. P.; Sattelmeyer, K. W.; Saunders, M.; Schaefer, H. F.; Schleyer, P. v. R. *J. Phys. Chem. A* **2006**, *110*, 4287.
- Naumkin, F. Y. *J. Phys. Chem. A* **2008**, *112*, 4660.
- Schreiner, P. R. *Angew. Chem., Int. Ed.* **2007**, *46*, 4217.
- Schreiner, P. R.; Fokin, A. A.; Pascal, R. A.; de Meijere, A. *Org. Lett.* **2006**, *8*, 3635.

- (57) Wodrich, M. D.; Corminboeuf, C.; Schleyer, P. v. R. *Org. Lett.* **2006**, *8*, 3631.
- (58) Check, C. E.; Gilbert, T. M. *J. Org. Chem.* **2005**, *70*, 9828.
- (59) Redfern, P. C.; Zapol, P.; Curtiss, L. A.; Raghavachari, K. *J. Phys. Chem. A* **2000**, *104*, 5850.
- (60) Frisch, M. J. In *Gaussian 03 Revision E.01*; Gaussian Inc.: Pittsburgh, PA, 2003.
- (61) Reed, A. E.; Curtiss, L. A.; Weinhold, F. *Chem. Rev.* **1988**, *88*, 899.
- (62) Weinhold, F.; Landis, C. R. *Valency and Bonding: A Natural Bond Orbital Donor-Acceptor Perspective*; Cambridge University Press: New York, 2003.
- (63) Boldyrev, A. I.; Wang, L. S. *J. Phys. Chem. A* **2001**, *105*, 10759.
- (64) Ghouri, M. M.; Yareeda, L.; Mainardi, D. S. *J. Phys. Chem. A* **2007**, *111*, 13133.
- (65) Wang, Z. X.; Schleyer, P. v. R. *J. Am. Chem. Soc.* **2001**, *123*, 994.
- (66) Wang, Z. X.; Zhang, C. G.; Chen, Z. F.; Schleyer, P. v. R. *Inorg. Chem.* **2008**, *47*, 1332.
- (67) Zubarev, D. Y.; Boldyrev, A. I. *J. Chem. Phys.* **2005**, *122*.
- (68) Greenwood, N. N.; Earnshaw, A. *Chemistry of the Elements*, 2nd ed; Elsevier, Ltd: Leeds, 1997.

JP8099187